Eng. Sci., 2021, **16**, 203–210

Engineered Science

DOI: https://dx.doi.org/10.30919/es8d560

Preparation and Characterization of Piezoelectric Foams Based on Cyclic Olefin Copolymer

Hui Wang, Xiaolin Wang, Zhe Liu, Mohammad Faisal Ahmed, Yan Li and Changchun Zeng*

Abstract

A series of cyclic olefin copolymer (COC) based piezoelectrets are fabricated using a carbon dioxide assisted assembly process followed by direct contact charging. The effects of both the piezoelectrets structure design parameters and the charging conditions on the piezoelectricity are studied. The piezoelectricity of the fabricated piezoelectrets is characterized by quasi-static piezoelectric coefficient d_{33}. The COC piezoelectrets show substantial piezoelectric activity, with d_{33} approaching up to 1100 pC/N. Moreover, the thermal stability of the COC piezoelectrets is investigated by thermally stimulated discharge. The COC show excellent thermal stability, with the d_{33} retaining over 80% of the initial value after annealed at 170 ºC. Hysteresis loop measurements are used to investigate the charge build up process inside the artificial void to obtain the critical breakdown voltage and quasi-permanent charges. The critical breakdown voltage is further modeled using the established layer model, which agreed well with the experimental measurements. With the superior thermal stability and significant piezoelectric sensitivity, the COC piezoelectrets demonstrated in the study may be valuable in a variety of applications, such as sensing, actuating, energy harvesting and many other fields.

Keywords: Piezoelectric polymer foam; Cyclic olefin copolymer; Piezoelectric activity; Electromechanical properties.
Received: 6 October 2021; Accepted: 30 October 2021.
Article type: Research article.

1. Introduction

Piezoelectric materials convert mechanical energy to electrical energy. Currently, the dominant commercialized piezoelectric materials are ceramic materials, such as lead zirconate titanate (PZT) ceramics. Polymer piezoelectrets (or polymer based piezoelectric foam) have been investigated in Finland since 1989.[1] Piezoelectrets are charged porous materials in which the piezoelectricity arises from the macro electric dipoles in the porous structure.[2-5] Through dielectric barrier discharge, charges of opposite signs are deposited on the top and bottom of the pores, forming macroscopic dipoles. Like traditional piezoelectric materials that have molecular dipoles, when deformed under an external force, the macroscopic dipoles also change, leading to induced external electrical signal. Compared to traditional piezoelectric materials, polymer piezoelectrets demonstrate advantages, such as flexibility, nontoxic, lightweight and low cost. A variety of potential applications are available for piezoelectrets, such as flexible electronics,[6,7] actuators,[1,8] acoustic transducers[9,10] and energy harvesters.[11-15]

A major concern for piezoelectrets is the relatively low thermal stability of the materials. For example, the most commercialized piezoelectret, polypropylene piezoelectret, has a working temperature of only about 70-80 ºC.[16, 17] Many materials have been explored to address this, including polyethylene terephthalate (PET),[18, 19] polyetherimide (PEI),[20,21] polycarbonate (PC),[20,22] polyethylene naphthalate (PEN),[23-26] fluorinated ethylene propylene (FEP),[27-36] polyethylene (PE),[37,38] polytetrafluoroethylene (PTFE)[30, 39-41] and polypropylene (PP).[10,17,42-46] Nevertheless, in most reported studies, the piezoelectric activity produced from these materials was not very high, and balanced mechanical and electromechanical properties were lacking. For example, fluorinated polymer piezoelectrets demonstrated good thermal stability and piezoelectric activity,[28] however, their low mechanical strength as well as creep behavior limited its application.

Cyclic olefin copolymer (COC) is a type of amorphous polymer made by chain copolymerization of cyclic monomers, such as norbornene or tetracyclododecene with ethene. COC has excellent processability, environmentally stable, low dielectric constant and low dielectric losses, excellent mechanical properties and particularly, outstanding thermal

Department of Industrial and Manufacturing, FAMU-FSU College of Engineering, High-Performance Materials Institute, Florida State University Tallahassee, FL 32310 USA.
**Email:* zeng@eng.famu.fsu.edu (C. Zeng)

stability. COC also exhibits excellent positive charge storage capabilities, which is crucial for piezoelectret's performance.[47] Several studies have been conducted on fabricating COC based piezoelectret.[48-51] Low piezoelectric activity was reported with the piezoelectric coefficient d_{33} typically less than 100 pC/N. This was mainly due the difficulty in achieving a structure with high porosity and low compression modulus. Previously, using a "non-overlapping" design that translate bending of structure unit into compression of the overall structure, we demonstrated it is possible to achieve a high d_{33} in COC piezoelectrets.[47]

Building on the results from the feasibility investigation, for this research we carried out a systematic study on the influences of the structure design, fabrication/assembly process, and charging conditions on the piezoelectric properties of the COC piezoelectret. Furthermore, the thermal stability of the COC piezoelectrets was studied. We further investigated the charge build up process by hysteresis loop analysis and the actuation behaviors of the materials by butterfly loop measurements. To our knowledge, this is the first comprehensive study on the fabrication and properties of COC piezoelectrets with substantial piezoelectric activity.

2. Material Fabrication and Experimental Details

2.1 Preparation of COC piezoelectret

The COC film used in this study was high-temperature grade COC film with a glass transition temperature of approximately 180 ºC (TOPAS 6017 purchased from TOPAS Advanced Polymers). Preparation of the piezoelectret were divided to three steps: (1) overall structure design and preparation, (2) assembly of the porous structure, and (3) charging of the porous structure to obtain piezoelectric activity.

Fig. 1a shows the schematic view of the overall sandwich structure of the COC piezoelectrets following the previously developed design principle.[47] The structure consisted of alternating solid COC films and films with rows of rectangular cavities (by laser machining) with predetermined widths and cavity-to-cavity distances. Fig. 1b shows the side view of a five-layer structure. The top, middle and bottom layers were solid films. The two porous layers were aligned in a way that the ridges of the layer above were positioned at the centerline of the rectangular cavities of the layer below. As previously reported.[47] compression of the structure resulted in the bending of the middle layer, leading to substantially higher overall compressive deformation and lower modulus of the piezoelectrets structure. Since the piezoelectric coefficient is inversely proportional to the elastic modulus,[52,53] this design should significantly increase the piezoelectric coefficient. The modulus of the structure can be tailored by varying the width of the cavity, cavity-to-cavity distance, number of layers, and the thickness of the layers. In the current study, we used the five-layer structure to conduct most of the investigation. The top and bottom layer was 101.6 μm thick, while the three middle layers were 50.8μm thick. Three different widths of the cavities of 2 mm, 2.5 mm and 3 mm were used to fabricate the structure.

In the second step, the layers were assembled into a monolithic structure using our previous developed supercritical CO_2 bonding technology.[47] Supercritical CO_2 bonding can significantly reduce both bulk and surface glass transition temperature of the polymers, as well as increase the chain mobility of molecules, enabling polymer films to be easily bonded together.[54,55] In our study, fusion/bonding of the structure with good dimension fidelity could occur at 120 ºC, which is approximately 60 ºC below the glass transition temperature of the COC. As an example, Fig. 1c shows the optical image of a fabricated piezoelectret with 3 mm cavity width. Unless otherwise noted, piezoelectrets with a five-layer structure and cavity width of 3mm were used for various electrical and electromechanical investigation. In the third step, the assembled structures were charged by contact using a Heinzinger PNC 1000-6 ump, after 2*2 cm^2 electrodes were sputter coated on both sides. Unless otherwise noted, a charging voltage of 5000 V was used.

2.2 Characterization of COC piezoelectret

2.2.1 Quasi-static piezoelectric coefficient

The sensitivity of the piezoelectrets is characterized by their piezoelectric coefficient, the amount of electrical charges being generated when a unit amount of force is applied (Pico Coulomb per Newton, or pC/N). Particularly, quasi-static piezoelectric coefficient is a common parameter to characterize the performance of piezoelectret, which was determined by:[52]

$$d_{33} = \frac{Q}{F} = \frac{\sigma}{p} \quad (1)$$

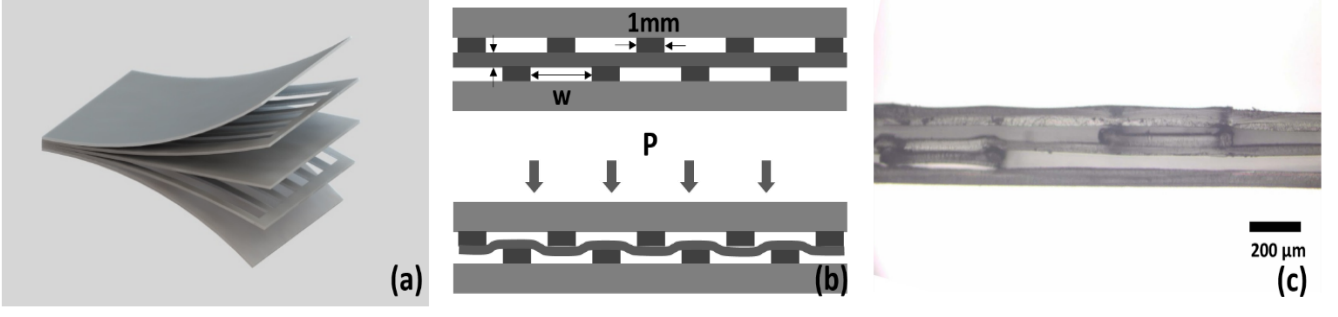

Fig. 1 (a). Schematic view of the prepared sandwich structure (b). Cross-section of the structure before and after compression (c). Optical image of piezoelectret (3mm channel width).

where d_{33} is quasi-static piezoelectric coefficient, Q is the amount of induced charge, F is applied force, σ is induced charge density, p is applied pressure. In the experiment, a 'preload' of 1.225 kPa was applied onto the sample to eliminate the artifacts from potential air gap between sample and electrode before testing. All types of prepared samples were measured by applying pressure from 2.45 kPa to 24.5 kPa. The induced charge was measured by an electrometer (Keithley 6517A). Samples were placed in aluminum foil for at least 24 hours before taking measurements.

2.2.2 Thermally stimulated discharge-current spectra

The thermal stability of the COC piezoelectret was characterized by thermally stimulated discharge (short circuit TSD spectra).[16,56] The temperature range was from room temperature to 240 ºC with a ramping rate of 3 ºC/min in a temperature-controlled furnace. Both sides of the sample were sputter coated with metal electrodes of 2×2 cm^2. The thermal stimulated current was recorded by an electrometer (Keithley 6517A).

2.2.3 Electrical hysteresis loop and voltage-displacement butterfly hysteresis loops (butterfly loop)

The charge or 'macro-dipole' build up process was investigated using hysteresis loop measurements using Precision Premier II (RADIANT) station connected to high voltage interface. Charging voltages with a range from 500 V to 7500 V were applied. The voltage-displacement butterfly hysteresis loops (butterfly loop), which can characterize the material actuation behavior, was also measured by the electric hysteresis loop testing equipment. Samples were firstly applied with a bipolar drive voltage with a maximum value of 8000 V. Small deformations of the material were then measured by a high precision optical fiber system (TF Analyzer 2000 system).

3. Results and Discussion

3.1 Quasi-static piezoelectric coefficient: effects of structure and processing parameters

3.1.1 Structure design

The quasi-static piezoelectric coefficient d_{33} of the COC piezoelectrets were measured. Fig. 2 shows the d_{33} of piezoelectrets with three different cavity widths. The piezoelectrets showed good to excellent piezoelectric sensitivity. A piezoelectric coefficient of about 1100 pC/N was realized at low pressures for samples with a cavity width of 3 mm. By varying the width of the cavity, the piezoelectric coefficient varied from about 350 pC/N to 1100 pC/N, and larger cavity widths resulted in higher piezoelectric activity. This can be understood since the deformation of the overall structure was dominantly contributed by the flexing of the middle layer (Fig. 1b), which can be regarded as a three or four-point bending. A larger cavity width, or a larger span in the bending configuration, would result in a larger bending deflection of the middle layer. This in turn would lead to a larger overall compressive strain of the piezoelectret structure and lower compressive modulus. Since the piezoelectric coefficient is inversely proportional to the modulus,[2,52,53], the increase of cavity width would resulted in an increase of the piezoelectric activity. The piezoelectric coefficient of the COC piezoelectrets in the current study (ranged from about 350 pC/N to 1100 pC/N, depending on the width of the cavity), are significantly higher than those reported in the literature (around 15pC/N) [49] and are comparable or better than the activity of the piezoelectrets made from PP.

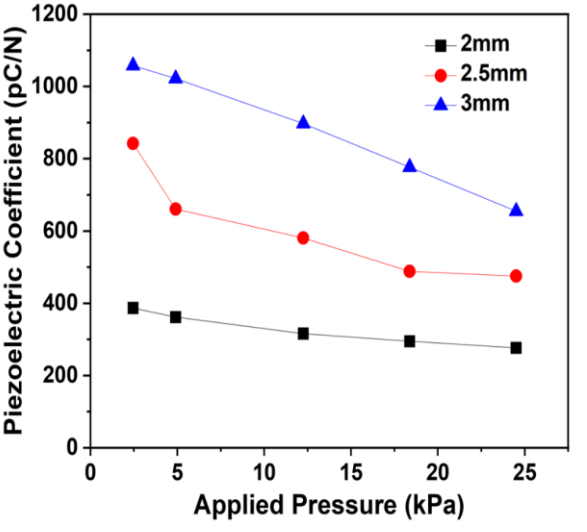

Fig. 2 Quasi-static piezoelectric coefficient of COC piezoelectrets with different cavity widths.

The non-overlapping design can be extended to beyond five layers to further tune the piezoelectric activity. To demonstrate this COC piezoelectrets with a nine-layer structure with the same geometric design was fabricated, and the piezoelectric activity was compared with that from 5-layer piezoelectrets. To ensure similar charging field strengths, the charging voltage of 10000V was used for the 9-layer piezoelectret, twice that for the 5-layer structure charging. Fig. 3 shows the results. The 9-layer piezoelectret showed higher piezoelectric sensitivity, particularly at low pressures. The improvement became less prominent with increasing pressure.

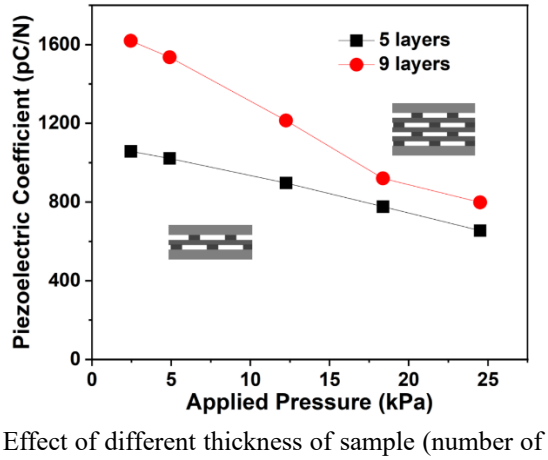

Fig. 3 Effect of different thickness of sample (number of layers) on piezoelectric coefficient.

3.1.2 Charging condition

Fig. 4 shows the results of the effects of the charging voltage on the quasi-static piezoelectric coefficient. Within the range of voltage used in the experiments, higher charging voltage resulted in higher piezoelectric coefficient d_{33}. In addition, the quasi-static piezoelectric coefficient was approximately linear to the charging voltage when the charging voltage is above the breakdown threshold voltage. This phenomenon will be discussed further later in the hysteresis loop analysis.

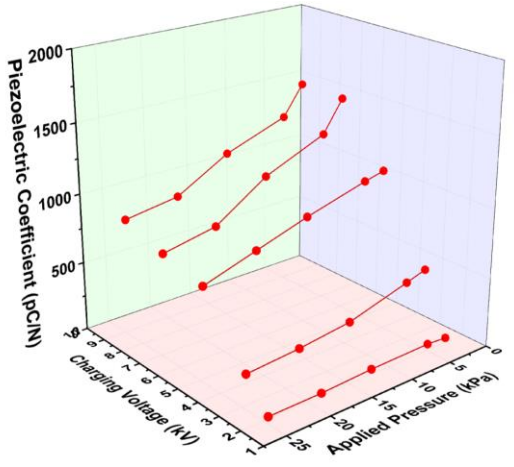

Fig. 4 Piezoelectric coefficient response to different charging voltage.

3.2 Electrical polarization and charge buildup in COC piezoelectret

The electrical polarization and actuation behavior of the COC piezoelectrets was investigated by hysteresis loop and butterfly loop tests. Fig. 5a shows the ac-bias voltage applied on the material over time. Fig. 5b shows the hysteresis loop of the experiment. Fig. 5c shows the quasi-permanent charge density in response to the maximum ac-bias voltage in the artificial void of the sample. No electric hysteresis loop was observed when the ac voltage was less than 2500 V, and 'macro-dipole' started to build up with an applied voltage of about 2500 V. Control experiments were also conducted on a COC solid of the same dimensions without artificial voids. The observed quasi-permanent charge was almost negligible. To ascertain the charging mechanism and predict the threshold charging voltage, an established analytical model[52,53] based on layered structure was employed. Fig. 6 shows the simplified model configuration consisting alternating layers of solid polymer layers and air gaps.

During contact charging, the electric field was built up. According to Gauss' theorem and Kirchhoff's second law:

$$\varepsilon_0 \varepsilon_{COC} E_{COC} = \varepsilon_0 E_{air} \quad (2)$$

$$E_{COC} h_{COC} + 2E_{air} h_{air} = V_{total} \quad (3)$$

where, ε_0 is dielectric permittivity of vacuum, ε_{COC} is relative permittivity of COC, h_{air} is the thickness of single air bubble height, and h_{COC} is total thickness of COC, E_{air} and E_{COC} are electric field strength in air and COC, respectively, and V_{total} is the applied voltage. According to the Paschen law, the critical breakdown electric field strength is determined by:

$$E_{bd} = \frac{ap}{\ln(pd)+b} \quad (4)$$

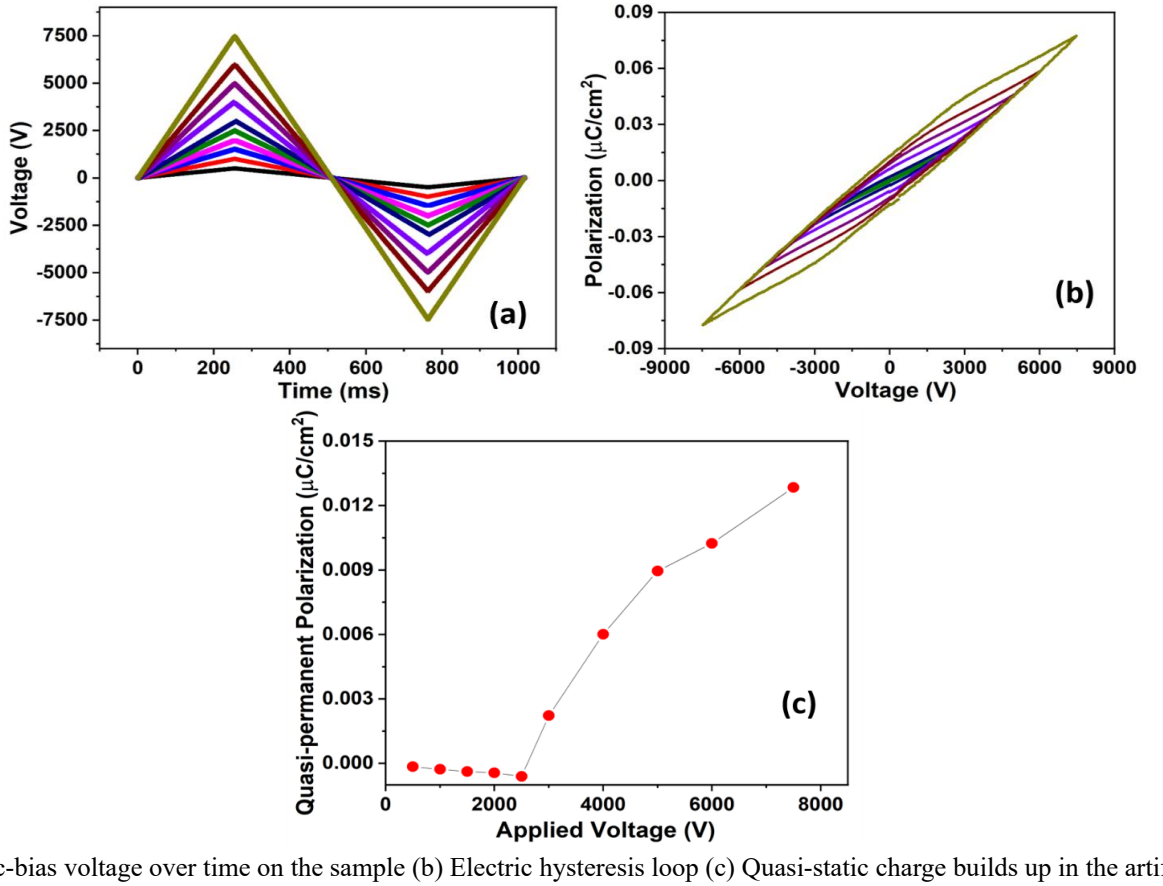

Fig. 5 (a) Ac-bias voltage over time on the sample (b) Electric hysteresis loop (c) Quasi-static charge builds up in the artificial void.

where, E_{bd} is the breakdown electric field strength, a is 4.36×10^7 V/(atm·m), p is pressure (1atm in the study), d is the thickness of gas (50.8 μm in this study), b equals to 12.8.

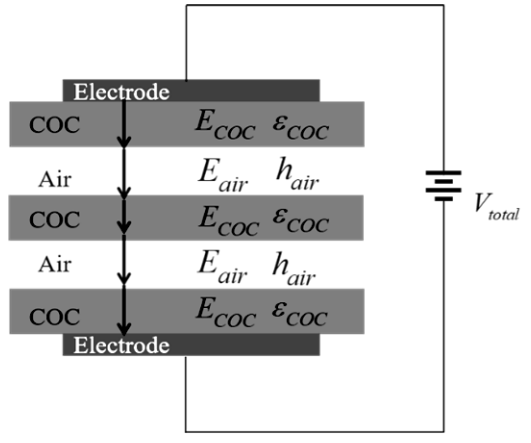

Fig. 6 Simplified model for calculating breakdown voltage.

From equations (2)-(4), the critical breakdown voltage can be determined by:

$$V_{bd} = \frac{ap}{\ln(ph_{air})+b}\left(\frac{h_{coc}}{\varepsilon_{coc}} + 2h_{air}\right) \quad (5)$$

The breakdown voltage thus calculated was 3141 V, higher than 2500 V observed in the experiment. This was the result of the slight deflection of the assembled structure and decrease of the void height during the CO_2 bond process (Fig. 1c). According to equation (5), a reduction of the air gaps thickness would result in a reduction of the breakdown voltage. Nevertheless, the model predicted breakdown voltage agreed reasonably well with experimental observations. Below the breakdown voltage (2500 V in experiments), nearly no charge was accumulated during the charging process. When the applied voltage was higher than the threshold breakdown voltage, a dielectric barrier discharge occurred, and a charge started to build up in the artificial void. The quasi-permanent charge density was approximately linearly proportional to the applied voltage after the applied voltage reached the threshold breakdown voltage (Fig. 1c). Back discharge, which may be caused by strong charge capturing capability of the materials, was not observed.

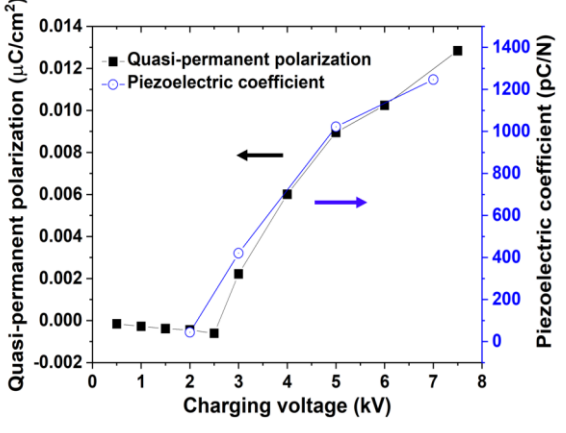

Fig. 7 Comparison and correlation between electrical polarization and quasi-static piezoelectric coefficient.

Fig. 7 shows the quasi-permanent polarization and quasi-static piezoelectric coefficients of COC piezoelectrets prepared under different charging voltages. Both followed similar trends against charging voltage (Fig. 7a), and the quasi-static piezoelectric coefficient was linearly related to the residual polarization (Fig. 7b). This can easily be understood since for piezoelectrets of the same structure and modulus, the piezoelectric coefficient would be linear to the surface charge inside the void ($d_{33} \propto \sigma$), which itself was linearly related to the residual polarization.

3.3 Thermal Stability of Electrical Charge and Piezoelectric d_{33}

To study the thermal stability of the COC piezoelectrets, TSD experiments were conducted, with Fig. 8a showing the results. The main discharge peak was located at approximately 210 ºC, indicating excellent thermal stability of the piezoelectrets. On the other hand, a moderate amount of discharge was still observed at the lower temperature region with the peak around 120 ºC. This peak (accounted for approximately 6%-14% of the total charge by integration of the current over time from measurements from multiple samples) may be the unstable charge inside the artificial void.

The discharges at low temperature may be related to the charge trapped in shallow energy well. To confirm this, annealing experiments were conducted. Samples were heated in an oven to 170 ºC and remained for 15 minutes, and TSD was measured (Fig. 8b). The samples were then cooled to room temperature, after which they were again heated from room temperature to 240 ºC for a second TSD. Fig. 8b shows the first TSD result – the annealing treatment during which "discrete discharge" was observed. After annealing, only negligible "discrete discharge" was observed, confirming the low temperature "discrete discharge" in the as-prepared piezoelectrets resulted from the emission of unstable charge. The result also suggests that two different charge storage mechanisms may exist in the COC piezoelectrets. After annealing the discharge peak temperature shifted to approximately 30 ºC higher, indicating that charges in the annealed sample were trapped in a deeper energy well. This phenomenon was also reported for other materials.[29]

Quasi-static piezoelectric coefficients were also measured before and after annealing. Fig. 8c shows the results. The quasi-static piezoelectric coefficient can maintain approximately 80% of its original value after annealing. The results suggest that the sample had an acceptable working temperature of approximately 170 ºC, at least for short term. Compared with the working temperature of PP foam with 70~80 ºC,[45] the COC based piezoelectrets exhibited vastly better thermal stability.

3.4 Voltage-displacement butterfly hysteresis loop and Actuation Behavior of COC Piezoelectrets

Fig. 9a shows the results of the actuation behavior of the piezoelectret, characterized by the butterfly loop measurement.

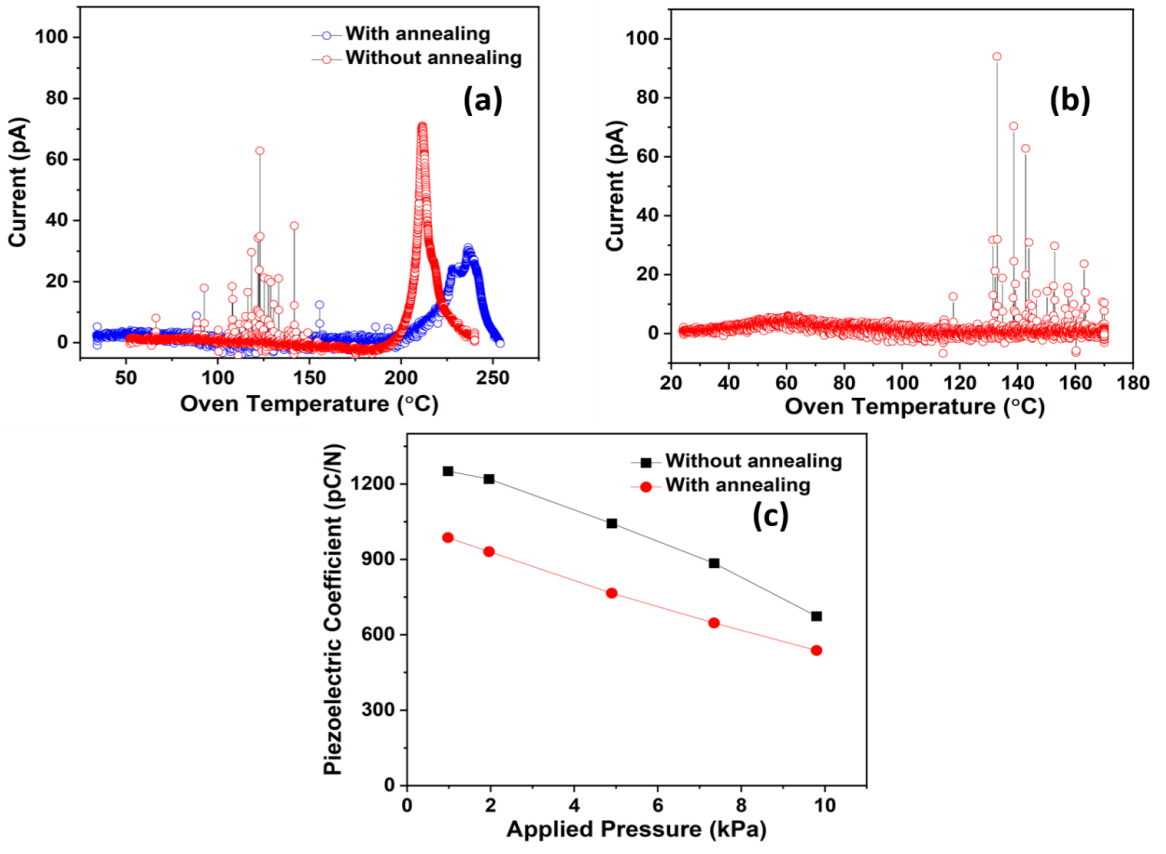

Fig. 8 (a) Thermally stimulated discharge spectrum of prepared piezoelectret with (blue) and without annealing (red); (b) TSD during annealing, pre-discharge; (c). Piezoelectric coefficient before and after annealing.

The inverse piezoelectric coefficient, calculated from measuring the slope of the butterfly loop from the origin point,[57,58] was 25 pm/V, which was considerably lower than the quasi-static piezoelectric coefficient.

Theoretically, for piezoelectric materials with microscopic dipoles, the piezoelectric coefficient and inverse piezoelectric coefficient should have the same value. On the other hand, the piezoelectric properties of the piezoelectrets originate from the macroscopic dipole of the artificial voids. The reason for the significant difference observed may be due to the differences in the response of the non-overlap structure to mechanical compression and electrical excitation. As previously discussed and also shown in Fig. 9b, the non-overlapping design allowed the mechanical force to be located at the center of the cavity to generate a large amount of flexing, which resulted in increased compression strains of the overall structure, decreased modules and increased piezoelectric activity. In the actuation mode, however, the force was generated by the applied electric field and exerted uniformly across the beam (assuming uniform distribution of surface charge in the voids). Therefore, the beam was effectively compressed instead of being bent during actuation. Such compression is futile in generating large deformation, leading to the substantially lower inverse piezoelectric coefficient.

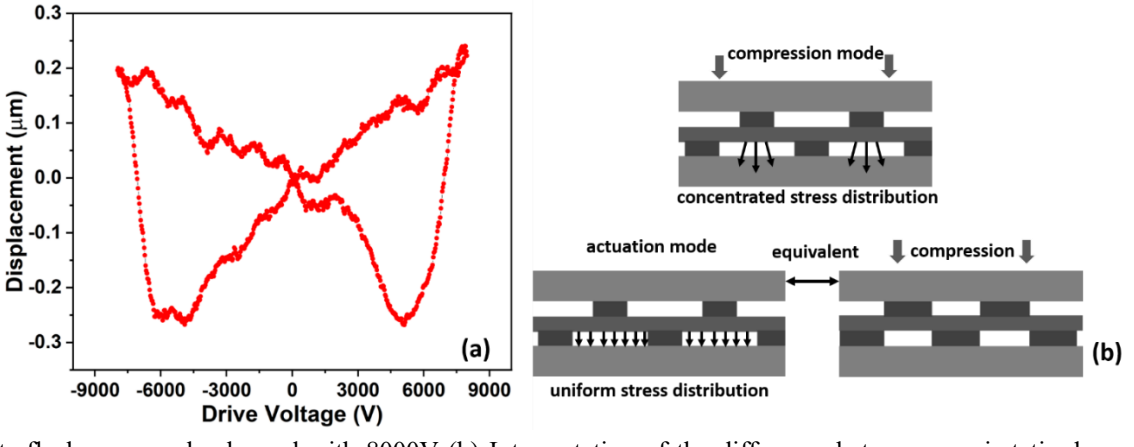

Fig. 9 (a) Butterfly loop, sample charged with 8000V (b) Interpretation of the difference between quasi-static d_{33} measurement condition and butterfly loop measurement condition.

While effective in improving piezoelectric sensing activity, the non-overlapping structure design has limitations and was ineffective in the actuation mode.

4. Conclusion

In this study, cyclic olefin copolymer (COC) based piezoelectrets were fabricated using different structural parameters and charging conditions. The charging process can be adequately described by the dielectric discharge and Paschen breakdown, and the experimentally observed breakdown voltage agreed reasonably well with prediction from the layer model. The COC piezoelectrets showed substantial piezoelectric activity, with d_{33} approaching up to 1100 pC/N. The COC piezoelectrets also exhibited excellent thermal stability, retaining over 80% of the initial piezoelectric activity after annealed at 170 ºC. The piezoelectrets showed different piezoelectric and inverse piezoelectric coefficient. This resulted from the difference in the response of the fabricated structures to mechanical and electrical forces, which itself is the result of the unique characteristic of the non-overlapping structure implemented in the piezoelectrets. With the high piezoelectric activity and thermal stability, the COC piezoelectrets may be suitable for a broad range of applications, particularly those at elevated temperatures.

Conflict of interest

There are no conflicts to declare.

Supporting information

Not applicable.

References

[1] A. Savolainen, K. Kirjavainen, *J. Macromol. Sci.*, 1989, **26**, 583-591, doi: 10.1080/00222338908051994.

[2] X. Qiu, *J. Appl. Phys.*, 2010, **108**, 011101, doi: 10.1063/1.3457141.

[3] M. Wegener, S. Bauer, *ChemPhysChem*, 2005, **6**, 1014-1025, doi: 10.1002/cphc.200400517.

[4] S. Bauer, R. Gerhard-Multhaupt, G. M. Sessler, *Phys.Today*, 2004, **57**, 37-43, doi: 10.1063/1.1688068.

[5] K. Sappati, S. Bhadra, *Sensors*, 2018, **18**, 3605, doi: 10.3390/s18113605.

[6] Y.-Y. Chiu, W.-Y. Lin, H.-Y. Wang, S.-B. Huang, M.-H. Wu, *Sensor. Actuat. A-Phys*, 2013, **189**, 328-334, doi: 10.1016/j.sna.2012.10.021.

[7] L. Ma, S. N. Melkote, J. B. Morehouse, J. B. Castle, J. W. Fonda, M. A. Johnson, *J. Intell. Mater. Syst. Struct.*, 2012, **23**, 1119-1130, doi: 10.1177/1045389x12443597.

[8] M. K. Hämäläinen, J. K. Parviainen, T. Jaaskelainen, *Rev. Sci. Instrum.*, 1996, **67**, 1598-1601, doi: 10.1063/1.1146867.

[9] Y. Xue, X. Zhang, R. Chadda, G. M. Sessler, M. Kupnik, *J. Acoust. Soc. Am.*, 2020, **147**, EL421-EL427, doi: 10.1121/10.0001274.

[10] J. Hillenbrand, G. M. Sessler, *J. Acoust. Soc. Am.*, 2004, **116**, 3267-3270, doi: 10.1121/1.1810272.

[11] J. Curie, P. Curie, *CR Acad. Bulg. Sci.*, 1881, **93**, 1137-1140.

[12] J. V. Turnhout, *Polym. J.*, 1971, **2**, 173-191, doi: 10.1295/polymj.2.173.

[13] X. Zhang, P. Pondrom, L. Wu, G. Sessler, *Appl. Phys. Lett.*, 2016, **108**, 193903, doi: 10.1063/1.4960480.

[14] G. Sessler, P. Pondrom, X. Zhang, *Phase Transit.*, 2016, **89**, 667-677, doi: 10.1063/1.5086113.

[15] P. Pondrom, J. Hillenbrand, G. M. Sessler, Bo, x, J. s, T. Melz, *IEEE Trans. Dielectr. Electr. Insul.*, 2015, **22**, 1470-1476, doi: 10.1109/TDEI.2015.7116339.

[16] M. Paajanen, J. Lekkala, K. Kirjavainen, *Sensor. Actuat. A-Phys*, 2000, **84**, 95-102, doi: 10.1016/S0924-4247(99)00269-1.

[17] M. Paajanen, J. Lekkala, H. Valimaki, *IEEE Trans. Dielectr. Electr. Insul.*, 2001, **8**, 629-636, doi: 10.1109/94.946715.

[18] W. Wirges, M. Wegener, O. Voronina, L. Zirkel, R. Gerhard-Multhaupt, *Adv. Funct. Mater.*, 2007, **17**, 324-329, doi: 10.1002/adfm.200600162.

[19] M. Wegener, W. Wirges, R. Gerhard-Multhaupt, *Adv. Eng. Mater.*, 2005, **7**, 1128-1131, doi: 10.1002/adem.200500177.

[20] N. Behrendt, *IEEE Trans. Dielectr. Electr. Insul.*, 2010, **17**, 1113-1122, doi: 10.1109/TDEI.2010.5539682.

[21] N. Behrendt, C. Greiner, F. Fischer, T. Frese, V. Altstädt, H. W. Schmidt, R. Giesa, J. Hillenbrand, G. M. Sessler, *Appl. Phys. A*, 2006, **85**, 87-93, doi: 10.1007/s00339-006-3660-7.

[22] X. Qiu, L. Holländer, R. F. Suárez, W. Wirges, R. Gerhard, *Appl. Phys. Lett.*, 2010, **97**, 072905, doi: 10.1063/1.3481802.

[23] F. Peng, H. Lars, W. Werner, G. Reimund, *Meas Sci Technol.*, 2012, **23**, 035604, http://stacks.iop.org/0957-0233/23/i=3/a=035604.

[24] F. Peng, Q. Xunlin, W. Wirges, R. Gerhard, L. Zirkel, *IEEE Trans. Dielectr. Electr. Insul.*, 2010, **17**, 1079-1087, doi: 10.1109/TDEI.2010.5539678.

[25] P. Fang, W. Wirges, M. Wegener, L. Zirkel, R. Gerhard, *e-Polymers*, 2008, **8**, 487-495, doi: 10.1515/epoly.2008.8.1.487.

[26] P. Fang, M. Wegener, W. Wirges, R. Gerhard, L. Zirkel, *Appl. Phys. Lett.*, 2007, **90**, 192908, doi: 10.1063/1.2738365.

[27] X. Zhang, G. M. Sessler, Y. Wang, *Int. J. Appl. Phys.*, 2014, **116**, 074109, doi: 10.1063/1.4893367.

[28] R. A. Pisani Altafim, D. Rychkov, W. Wirges, R. Gerhard, H. C. Basso, R. A. Correa Altafim, M. Melzer, *IEEE Trans. Dielectr. Electr. Insul.*, 2012, **19**, 1116-1123, doi: 10.1109/TDEI.2012.6259978.

[29] Z. Sun, X. Zhang, Z. Xia, X. Qiu, W. Wirges, R. Gerhard, C. Zeng, C. Zhang, B. Wang, *Appl. Phys. A*, 2011, **105**, 197-205, doi: 10.1007/s00339-011-6481-2.

[30] X. Zhang, G. Cao, Z. Sun, Z. Xia, *J. Appl. Phys.*, 2010, **108**, 064113, doi: 10.1063/1.3482011.

[31] R. A. P. Altafim, X. Qiu, W. Wirges, R. Gerhard, R. A. C. Altafim, H. C. Basso, W. Jenninger, J. Wagner, *J. Appl. Phys.*, 2009, **106**, 014106, doi: 10.1063/1.3159039.

[32] O. Voronina, M. Wegener, W. Wirges, R. Gerhard, L. Zirkel, H. Münstedt, *Appl. Phys. A*, 2008, **90**, 615-618, doi: 10.1007/s00339-007-4371-4.

[33] J. Huang, X. Zhang, Z. Xia, X. Wang, *J. Appl. Phys.*, 2008, **103**, 084111, doi: 10.1063/1.2910773.

[34] X. Zhang, J. Hillenbrand, G. M. Sessler, *J. Appl. Phys.*, 2007, **101**, 054114, doi: 10.1063/1.2562413.

[35] R. A. C. Altafim, H. C. Basso, R. A. P. Altafim, L. Lima, C. V. de Aquino, L. G. Neto, R. Gerhard-Multhaupt, *IEEE Trans. Dielectr. Electr. Insul.*, 2006, **13**, 979-985, doi: 10.1109/TDEI.2006.247822.

[36] X. Zhang, P. Pondrom, G. M. Sessler, X. Ma, *Nano Energy*, 2018, **50**, 52-61, doi: 10.1016/j.nanoen.2018.05.016.

[37] B. Gustavo Ortega, S. Pedro Llovera, M. Francisco, Q. Alfredo, *J. Phys. Conf. Ser.,* 2011, **301**, 012054, http://stacks.iop.org/1742-6596/301/i=1/a=012054.

[38] O. Hamdi, F. Mighri, D. Rodrigue, *Polym. Adv. Technol.* 2019, **30**, 153-161, doi: 10.1002/pat.4453.

[39] X. Zhang, X. Zhang, M. S. Gerhard, G. Xiangshan, *J. Phys. D Appl. Phys.*, 2014, **47**, 015501, http://stacks.iop.org/0022-3727/47/i=1/a=015501.

[40] X. Zhang, X. Zhang, G.M. sessler, G. xiangshan, *2013 IEEE Conference on Electrical Insulation and Dielectric Phenomena*, 2013, 579-582, doi: 10.1109/CEIDP.2013.6748276.

[41] R. Gerhard-Multhaupt, W. Kunstler, T. Gome, A. Pucher, T. Weinhold, M. Seiss, X. Zhongfu, A. Wedel, R. Danz, *IEEE Trans. Dielectr. Electr. Insul.*, 2000, **7**, 480-488, doi: 10.1109/94.868065.

[42] R. H. Ali Samadi, Taher Azdast, Hossein Abdollahi, Payam Zarrintaj & Mohammad Reza Saeb, *J. Macromol. Sci. Phys.*, 2020, **59**, 14, doi: 10.1080/00222348.2020.1730573.

[43] X. Zhang, X. Zhang, Q. You, G. M. Sessler, *Macromol. Mater. Eng.*, 2014, **299**, 290-295, doi: 10.1002/mame.201300161.

[44] X. Zhang, J. Huang, J. Chen, Z. Wan, S. Wang, Z. Xia, *Appl. Phys. Lett.*, 2007, **91**, 182901, doi: 10.1063/1.2803316.

[45] A. Mellinger, M. Wegener, W. Wirges, R. R. Mallepally, R. Gerhard-Multhaupt, *Ferroelectrics*, 2006, **331**, 189-199, doi: 10.1080/00150190600737933.

[46] G. S. Neugschwandtner, R. Schwödiauer, M. Vieytes, S. Bauer-Gogonea, S. Bauer, J. Hillenbrand, R. Kressmann, G. M. Sessler, M. Paajanen, J. Lekkala, *Appl. Phys. Lett.*, 2000, **77**, 3827-3829, doi: 10.1063/1.1331348.

[47] Y. Li, C. Zeng, *Macromol. Chem. Phys.*, 2013, **214**, 2733-2738, doi: 10.1002/macp.201300440.

[48] G. C. Montanari, D. Fabiani, F. Ciani, A. Motori, M. Paajanen, R. Gerhard-Multhaupt, M. Wegener, *IEEE Trans. Dielectr. Electr. Insul.*, 2007, **14**, 238-248, doi: 10.1109/TDEI.2007.302892.

[49] E. Saarimaki, M. Paajanen, A. M. Savijarvi, H. Minkkinen, M. Wegener, O. Voronina, R. Schulze, W. Wirges, R. Gerhard-Multhaupt, *IEEE Trans. Dielectr. Electr. Insul.*, 2006, **13**, 963-972, doi: 10.1109/TDEI.2006.247820.

[50] M. Wegener, M. Paajanen, O. Voronina, R. Schulze, W. Wirges, R. Gerhard-Multhaupt, *2005. ISE-12. 2005 12th International Symposium on Electrets*, 2005, 47-50, doi: 10.1109/ISE.2005.1612315.

[51] A.M. Savijarvi, M. Paajanen, E. Saarimaki, H. Minkkinen, *ISE-12. 2005 12th International Symposium on Electrets*, 2005, 75-78, doi: 10.1109/ISE.2005.1612322.

[52] G. M. Sessler, J. Hillenbrand, *Appl. Phys. Lett.*, 1999, **75**, 3405-3407, doi: 10.1063/1.125308.

[53] J. Hillenbrand, G. M. Sessler, *IEEE Trans. Dielectr. Electr. Insul.*, 2000, **7**, 537-542, doi: 10.1109/94.868074.

[54] Y. Yang, Y. Xie, X. Kang, L. J. Lee, D. A. Kniss, *Journal of the American Chemical Society*, 2006, **128**, 14040-14041, doi: 10.1021/ja066157u.

[55] Y. Yang, D. Liu, Y. Xie, L. J. Lee, D. L. Tomasko, *Adv. Mater.*, 2007, **19**, 251-254, doi: 10.1002/adma.200601481.

[56] C. Gongxun, Z. Xiaoqing, Z. Da, C. Zhang, W. Ben, Z. Changchun, *IEEE Trans. Dielectr. Electr. Insul.*, 2012, **19**, 1108-1115, doi: 10.1109/TDEI.2012.6259977.

[57] S. Xie, A. Gannepalli, Q. N. Chen, Y. Liu, Y. Zhou, R. Proksch, J. Li, *Nanoscale*, 2012, **4**, 408-413, doi: 10.1039/C1NR11099C.

[58] M. Hinterstein, J. Rouquette, J. Haines, P. Papet, M. Knapp, J. Glaum, H. Fuess, *Phys. Rev. Lett.*, 2011, **107**, 077602, doi: 10.1103/PhysRevLett.107.077602.

